NACA RM A54A07

C. 2

NACA

RESEARCH MEMORANDUM

EFFECTS OF BASE BLEED ON THE BASE PRESSURE OF BLUNT-TRAILING-EDGE AIRFOILS AT SUPERSONIC SPEEDS

By William R. Wimbrow

Ames Aeronautical Laboratory
Moffett Field, Calif.

NATIONAL ADVISORY COMMITTEE
FOR AERONAUTICS

WASHINGTON
March 25, 1954

NACA RM A54A07

NATIONAL ADVISORY COMMITTEE FOR AERONAUTICS

RESEARCH MEMORANDUM

EFFECTS OF BASE BLEED ON THE BASE PRESSURE OF BLUNT-TRAILING-EDGE AIRFOILS AT SUPERSONIC SPEEDS

By William R. Wimbrow

SUMMARY

The effect on base pressure of bleeding air to the semidead-air region at the trailing edge of two-dimensional blunt-trailing-edge airfoils has been investigated at Mach numbers of 1.5 and 2.0. Variable base bleed was provided from an external air supply. The variation of base pressure with base-bleed rate was determined for two airfoil profiles with both laminar and turbulent boundary layers approaching the trailing edge. The effects of varying the cross-sectional area and location of the base-bleed nozzles were also investigated. It was found that the maximum reduction in base drag was obtained when the total pressure of the bleed air was 75 to 90 percent of the ambient static pressure. Reductions in base drag of the order of 50 percent were measured.

INTRODUCTION

It has been shown that at supersonic speeds a properly designed blunt-trailing-edge airfoil can have less drag and a greater lift-curve slope than a sharp-trailing-edge airfoil having the same strength or stiffness. (See refs. 1 and 2.) When such an airfoil is submerged in a supersonic stream, a semidead-air region is created at the trailing edge, and the pressure in this region is generally lower than the ambient static pressure. The pressure drag of the surface wetted by this semidead-air region is commonly referred to as "base drag." This base drag, in an extreme case, can account for as much as 80 percent of the total drag of a blunt-trailing-edge airfoil. If the base drag could be decreased by increasing the base pressure, the superiority of a blunt-trailing-edge airfoil would be more pronounced and would extend over a wider Mach number range.

In reference 3, Cortright and Schroeder present the results of a preliminary study of a technique to reduce the base drag of blunt-base bodies of revolution which they call base bleed. Relatively small amounts of air were allowed to bleed into the semidead-air region at the base of the bodies. Base-drag reductions as high as 32 percent and total drag reductions as high as 7 percent were measured although no great effort was made to optimize the geometry of the ducts and nozzles employed.

The present investigation was undertaken to determine the effectiveness of the base-bleed technique when applied to blunt-trailing-edge airfoils. The objectives of the investigation were to determine how base pressure varied with bleed rate and how this relationship was influenced by jet geometry, airfoil profile, the type of boundary layer approaching the trailing edge, Reynolds number, and angle of attack. This information would allow an evaluation of the usefulness of the base-bleed technique and provide the basis for the preliminary design of practical base-bleed installations for airfoils.

SYMBOLS

A_b	area of the base of the blunt-trailing-edge airfoil
A_j	exit area of the base-bleed nozzle
c	airfoil chord
c_d	section drag coefficient
c_{d_o}	section drag coefficient without base bleed
c_{d_b}	section base drag coefficient, $\frac{p_\infty - p_b}{q} \frac{h_b}{c}$
$c_{d_{b_o}}$	section base drag coefficient without base bleed
h_b	trailing-edge thickness
h_i	vertical height of the scoop inlet
m_j	mass-flow rate through the base-bleed nozzles
m_∞	free-stream mass-flow rate through an area equal to the area of the base of the blunt-trailing-edge airfoil
M_∞	free-stream Mach number

p_b base pressure

p_c plenum-chamber pressure or total pressure of the base-bleed air jets

p_j static pressure at the throat of the base-bleed nozzles

p_∞ free-stream static pressure

q free-stream dynamic pressure

R Reynolds number based on the airfoil chord

APPARATUS AND TEST METHODS

Wind Tunnel

The experimental investigation was conducted in the Ames 1- by 3-foot supersonic wind tunnel No. 1. This wind tunnel is of the closed-circuit, continuous-operation type and is equipped with a flexible-plate nozzle that provides a variation of Mach numbers from 1.2 to 2.2. The total pressure in the tunnel can be varied to provide Reynolds numbers from 0.8 to 6.8 million per foot of model length. The water content of the air is maintained at less than 0.0003 pound of water per pound of dry air; consequently, the effect of humidity on the flow is negligible.

Two-Dimensional Channel

The airfoil models employed in this investigation were tested in a two-dimensional channel as shown in figure 1. The channel consisted essentially of two vertical flat plates between which airfoil models could be mounted horizontally. The plates were suspended in the test section of the wind tunnel in such a manner that the boundary layer on each side wall of the tunnel passed between the plate and the tunnel wall. The models were mounted between turntables in the plates so that the angle of attack could be varied. Optical glass windows were provided in these turntables and in the wind-tunnel walls. The struts supporting the vertical plates were so arranged that the disturbances created by them did not pass through the field of vision of the windows. However, the bleed-air supply line passed through the boundary-layer passage on the south side of the tunnel directly upstream of the window axis. The wake from this supply line would interfere with the normal use of a schlieren apparatus. Therefore, the optical glass window in the turntable through which the supply line passed was replaced with a ground glass window. Then, when the parallel light beam from the schlieren

light source passed through the test section from the north side, a shadowgraph image of the flow around the base of the airfoil model appeared on the ground glass. This image could be photographed from the south side of the tunnel without distortion by the wake from the air supply line.

Models

Two 10-percent-thick airfoil models having chord lengths of 6 inches were employed in this investigation. One model had a span of 6 inches and a trailing-edge thickness equal to the maximum thickness. This model, hereafter referred to as the "full-blunt" airfoil, is shown in figure 2(a). The other model had a span of 4 inches and a trailing-edge thickness equal to one-half the maximum thickness. This model is referred to as the "half-blunt" airfoil and is shown in figure 2(b). Both models were constructed from steel and were made hollow to provide a plenum chamber for the bleed air. Air ducts, made integral with the airfoil, extended through the vertical plate at one end of the models and connected with the bleed-air supply line at the wind-tunnel wall.

The airfoil models were made with interchangeable brass blocks at the trailing edge, as shown in figure 2. These blocks contained the base-bleed nozzles and the orifices for measuring the base pressure and the static pressure at the throat of the nozzles. Thin-wall stainless-steel tubing was connected to the pressure measuring orifices and passed through the plenum chamber and the air supply line to the outside of the tunnel.

Because of the small scale of the tests, it was necessary to employ a boundary-layer trip to obtain extensive runs of turbulent boundary layer. For this purpose, a wire with a diameter of 0.006 inch was stretched across the upper and lower surfaces of the airfoil models, approximately 3/4 inch from the leading edge.

Procedure

Dry air for the base-bleed system was taken from the storage tank of the wind-tunnel make-up air system. This air was passed through a pressure regulator that enabled the operator to select and then hold a constant plenum-chamber pressure. The variation of base pressure with chamber pressure was measured with a multiple-tube manometer with an atmospheric sump. With the models removed from the wind tunnel, the pressure at the position normally occupied by the trailing edge of the airfoils was measured to determine the tunnel-empty static pressure relative to the total pressure of the air stream. All the base-pressure

[redacted]

and chamber-pressure measurements are expressed in terms of this tunnel-empty static pressure.

The base pressure and the jet static pressure were measured at various locations, as shown in figure 2. The plenum-chamber pressure was measured at two spanwise stations. By comparison of the measurements at the various stations, it was possible to determine if the flow through the nozzles were uniform across the span of the airfoil and if the pressure were uniform over the base.

The full-blunt airfoil and its nozzle blocks were constructed and tested first at nominal Mach numbers of 1.5 and 2.0. It soon became evident that the largest nozzles gave the greatest increase in base pressure. In an effort to determine if there were an upper limit to this trend, the area of the nozzle was progressively increased. When the ratio of jet area to base area exceeded approximately 0.25, however, the air-supply duct was no longer large enough in relation to the size of the nozzle to provide uniform flow through the nozzle across the span of the model. The half-blunt airfoil was then designed and constructed to remedy this situation. As shown in figure 2, the base of the half-blunt airfoil was one-third as large as the base of the full-blunt airfoil, while the size of the air-supply duct was approximately the same in both cases.

The half-blunt airfoil was tested with the nozzle blocks having the larger jet areas at a nominal Mach number of 2.0. This airfoil was tested with and without the boundary-layer trip wire. The effects of Reynolds number and angle of attack were also investigated with this airfoil.

RESULTS AND DISCUSSION

The results of the investigation of the variation of base pressure with base-bleed rate are presented in figures 3 through 7. Since the base pressure was always essentially uniform across the base of the airfoil from top to bottom and was usually uniform in a spanwise direction, the individual base-pressure measurements have been averaged. The ratio of the average base pressure to free-stream static pressure $\bar{p}_b/p_\infty$ is plotted against the ratio of the plenum-chamber pressure to the free-stream static pressure p_c/p_∞. Since the rate of flow of bleed air is a function of the difference between the plenum-chamber pressure and the base pressure, the chamber-pressure ratio is probably not the best independent variable that could be used. The data are presented in this form, however, because such a plot gives a direct indication of the optimum pressure level required at the source of the bleed air and thereby aids in selecting the best air source for a particular application of the base-bleed technique. The lowest value of the chamber-pressure ratio

presented corresponds to no flow through the base-bleed nozzles and is referred to as the initial base pressure. The data points corresponding to subsonic flow through the nozzles across the entire span are indicated by filled symbols on all the figures.

Effects of Jet Geometry

The first phase of the investigation was concerned with the variation of base pressure with plenum-chamber pressure for various nozzle configurations with approximately the same total jet area. Figure 3(a) presents the results obtained with the full-blunt airfoil at a Mach number of 1.5. The boundary layer was turbulent and the ratio of the area of the jets to the area of the base of the airfoil was approximately 5 percent. The results obtained with the half-blunt wing at a Mach number of 2.0 and an area ratio of 50 percent are shown in figure 3(b) for a turbulent boundary layer and in figure 3(c) for a laminar boundary layer. The geometry of the various nozzle blocks employed is shown in the figures. In all cases, the base pressure increased as the chamber pressure was increased until a maximum or peak base pressure was reached. This peak pressure occurred when the chamber-pressure ratio was between 0.75 and 0.95. Beyond this point, the base pressure, in general, decreased with further increases in chamber pressure, but the various nozzle blocks exhibited widely varying behavior. However, this portion of the curve is of little interest here since the success of the base-bleed technique depends on realizing worthwhile drag reductions with the relatively small quantities of bleed air required to obtain the peak base pressure.

Inspection of figure 3 shows that the peak pressure was generally a little higher for the nozzle configurations that discharge air near the upper and lower edges of the base than it was for the configurations with the jet at the center of the base. The multiple-jet configuration shown in figures 3(b) and 3(c) appears to be slightly superior to the others tested in that the peak base pressure was at least as high as any, and the curve was relatively flat in the vicinity of the peak. This latter characteristic would be desirable since it would provide near-optimum drag reduction without critical control of the chamber pressure. However, the double-jet configuration was selected for further investigation because nozzle blocks of this general geometry were simpler to construct than the multiple-jet arrangements. As shown in figure 2, the jets of the double-jet nozzle blocks for the half-blunt airfoil extended all the way to the upper and lower edges of the airfoil base and formed a sharp edge, while those for the full-blunt airfoil did not. It is not known whether this difference in detail has any effect on the results.

Effects of Jet Area

The effect of varying the cross-sectional area of the discharge jets was investigated with a series of nozzle blocks having two jets, one at the upper edge of the base and one at the lower edge. The results are presented in figure 4. In general, it can be seen that the plenum-chamber pressure required to obtain the peak base pressure is essentially independent of the area of the jet. However, the magnitude of the peak pressure increases as the area of the jet increases.

The data obtained with the boundary-layer trip on the full-blunt airfoil at a Mach number of 1.5 are shown in figure 4(a). It can be seen that a sudden decrease in base pressure occurred as the chamber-pressure ratio was increased beyond 1.0 for the nozzle blocks with jet-area ratios of 2.7, 5.3, and 10.7 percent. Inspection of the shadowgraph pictures and the jet static-pressure measurements indicates that this sudden drop in base pressure occurred when the bleed air attained sonic velocity in the nozzle. For the nozzle block with a jet-area ratio of 21.3 percent, however, the decrease in base pressure beyond the peak value is much more gradual. Comparison of the pressure measurements from the three spanwise stations for the different nozzle blocks revealed that for the smaller area ratios the flow through the nozzles was uniform across the span of the model at all chamber pressures. For the nozzle block with an area ratio of 21.3 percent, the flow was uniform only for chamber pressures below that corresponding to the peak base pressure. As the chamber pressure was increased beyond this value, the flow became progressively more nonuniform and the air attained sonic velocity first at the side of the model nearest the air supply line and then progressively across the span. This nonuniformity of the air flow through the nozzle resulted in a spanwise variation of the base pressure, which was not nearly so pronounced as was the spanwise variation in the jet static pressure. The fact that the flow through the largest nozzle did not attain sonic velocity uniformly probably accounts for the more gradual drop in base pressure.

The data shown in figure 4(b) were also obtained with the boundary-layer trip on the full-blunt airfoil, but at a Mach number of 2.0. They exhibit the same trends as those in figure 4(a) except that there is no sudden drop in base pressure for the nozzle block with a jet-area ratio of 2.7 percent although the flow through the nozzle was sonic for chamber-pressure ratios greater than 1.2. It can be seen that for all of the nozzle blocks tested at this Mach number, the base pressure is greater when the chamber-pressure ratio exceeds 1.2 than it is with no base bleed. This is in direct contrast to the situation at a Mach number of 1.5 (see fig. 4(a)). Evidently, the peak pressure for a jet-area ratio of 2.7 percent is of the same order of magnitude as the base pressure with sonic flow through the nozzle and, hence, there was no sudden drop in base pressure for this nozzle block.

The results obtained with a boundary-layer trip on the half-blunt airfoil at a Mach number of 2.0 are shown in figure 4(c) and the results obtained without the boundary-layer trip are shown in figure 4(d). As was the case with the full-blunt airfoil, the peak base pressure continued to increase as the jet-area ratio was increased. However, the sudden drop in base pressure beyond the peak value did not take place in spite of the fact that, for the 25-percent jet-area ratio at least, the ratio of jet area to supply line area was reasonably small. Inspection of the spanwise pressure distributions revealed that the flow through the nozzle was essentially uniform across the span of the model for all three nozzle blocks when the chamber-pressure ratio was less than 0.90. As the chamber-pressure ratio was increased beyond 0.90, the flow became slightly nonuniform and the jets attained sonic velocity progressively across the span. As the chamber-pressure ratio was increased beyond 2.0, the flow through the nozzles of the 25- and 50-percent-area-ratio blocks became essentially uniform again. The flow through the 75-percent-area-ratio block remained slightly nonuniform at all values of chamber-pressure ratio above 0.90. The only essential difference between the results for laminar and turbulent boundary layers was that the initial base pressure with no base bleed was slightly higher when the boundary layer was laminar.

Effect of Base Bleed on the Flow in the Wake

Two typical sets of shadowgraph pictures of the wake behind the half-blunt airfoil with base bleed are shown in figures 5 and 6. These pictures were obtained at a free-stream Mach number of 2.0, a Reynolds number of 3.1 million, and with the boundary-layer trip wire. Figure 5 shows the wake with a single base-bleed jet located midway between the upper and lower edges of the base. Figure 6 shows the wake with two base-bleed jets that discharge air at the upper and lower edges of the base. In both cases the jet area is 50 percent of the base area. The variation of average base pressure with plenum-chamber pressure for the configurations in question is also shown in figures 5 and 6. The letter at each data point identifies the shadowgraph picture taken at that point.

With no base bleed, a semidead-air region is created at the trailing edge of the wing. The boundaries of this region are visible in the shadowgraph pictures. Along these boundaries a mixing process takes place that acts essentially like a pump. This mixing process reduces the pressure in the dead-air region until the pumping capacity of the process is reached. Bleeding additional low-velocity air to this region from the base of the wing increases the demands on the pumping capacity of the mixing process and, for a given base-bleed rate, the system attains equilibrium at a higher pressure level than it does without base bleed. Thus, as the chamber pressure is increased, the flow rate of the bleed air is increased and, therefore, the base pressure is increased. As can

be seen in the shadowgraph pictures, the increase in base pressure decreases the convergence of the wake and causes the trailing shock wave to decrease in intensity. This trend continues as long as the velocity at which the bleed air enters the semidead-air region is subsonic.

As the chamber pressure is increased further and the air flowing through the nozzle approaches sonic velocity, the base pressure reaches a maximum and then begins to decrease. Two different types of behavior were observed for this decrease in base pressure, as illustrated in figure 7. For the smaller nozzles, a sudden, almost discontinuous drop in base pressure occurred, as shown in figure 7(a). For the larger nozzles, the base pressure decreased gradually as shown in figure 7(b). In addition to the base pressure, the variation of the average static pressure at the throat of the nozzle p_j is also shown in figure 7. When the ratio p_j/p_c decreases to 0.528, sonic flow is established in the throat and, theoretically, this ratio remains constant for further increases in chamber pressure. It is apparent from the data presented in figure 7 that the decrease in base pressure is associated with the establishment of sonic flow in the nozzles. When the sudden drop in base pressure was observed, p_j was always uniform across the span of the airfoil. When the gradual decrease was observed, p_j as measured on the side of the airfoil next to the air supply line reached the critical value at a lower chamber pressure than did p_j as measured at the opposite side of the airfoil. In all the figures, the filled symbols indicate data that were obtained with subsonic flow across the entire span.

As the chamber pressure was increased still further, the air issuing from the nozzle expanded to supersonic speeds in a free jet. Eventually, the closed parts of the base are bounded on both sides by supersonic streams. For the data shown in figure 5, this type of flow existed at chamber-pressure ratios greater than approximately 2.2, but it is not clear just where it started in figure 6. In this range, the base pressure can evidently increase or decrease with further increase in chamber pressure, depending on the height of the closed part of the base and the geometry of the base-bleed nozzles.

Effect of Angle of Attack

Several of the configurations were tested at angles of attack of 5° and 10° in addition to the tests at 0°. Typical results are shown in figure 8. It can be seen that changes in angle of attack of the order of 5° have very little effect on the variation of base pressure with chamber pressure. The data obtained at 10° angle of attack, however, show a lower base pressure at any given chamber-pressure ratio below 2.0.

However, the change in base pressure due to base bleed appears to be essentially independent of angle of attack.

Effect of Reynolds Number

The effect of Reynolds number on the variation of base pressure with chamber pressure was investigated for several of the nozzle-block configurations. When transition to turbulent flow in the boundary layer was fixed with the trip wire, varying Reynolds numbers from 2.3 to 3.4 million had a negligible effect on the variation of base pressure with chamber pressure. Under these conditions the initial base pressure without base bleed was also independent of Reynolds number, as would be expected from previous investigations.

Typical results obtained without the boundary-layer trip wire are shown in figure 9. With no base bleed, the base pressure decreased with increasing Reynolds number which is also in agreement with previous investigations for laminar boundary-layer flow. In contrast to the effect of angle of attack, however, for a given chamber pressure, the base pressure was essentially independent of Reynolds number even though the initial base pressure varied with Reynolds number. Furthermore, the base pressure corresponding to a given chamber pressure appears to be independent of whether the boundary layer approaching the trailing edge is laminar or turbulent as long as the flow through the jet is subsonic. For example, the boundary layer appeared to be turbulent in the shadowgraph pictures corresponding to the data shown in figure 9 for a Reynolds number of 3.43 million and, also, these data agree with those obtained with the boundary-layer trip.

Correlation of the Results With Mass-Flow Rate of the Bleed Air

Figure 10 presents an attempt to correlate all of the results obtained with the double-jet nozzle blocks. The change in base-pressure ratio due to base bleed is plotted against the ratio of the mass-flow rate of the bleed air to the free-stream mass-flow rate through an area equal to the area of the airfoil base. The mass-flow rate of the bleed air was determined by measuring the plenum-chamber pressure and the static pressure at the point of minimum cross-sectional area of the base-bleed nozzles. No allowance was made in the resulting calculations for the boundary layer in the nozzles and the accuracy of the resulting mass-flow rate is known to be poor.

Inspection of figure 10 reveals that a crude correlation exists if only the data points corresponding to subsonic flow through the nozzles

(indicated by filled symbols) are considered. The results obtained with different jet-area ratios correlate only very roughly for each of the test conditions illustrated. Comparison of figures 10(b) and 10(c) indicates that the correlation approximately accounts for variations in the ratio of the trailing-edge thickness to the maximum thickness of the wing. However, comparison of figures 10(a) and 10(b) indicates that the data obtained at a Mach number of 2.0 do not follow exactly the same trend as those obtained at a Mach number of 1.5 and, hence, the correlation may be even less satisfactory for a wider range of Mach numbers. Comparison of figures 10(c) and 10(d) reveals that the correlation is also relatively poor when both laminar and turbulent boundary layers are considered. Since it has been shown earlier that the change in base pressure due to base bleed is independent of Reynolds number when the boundary layer is turbulent but depends on Reynolds number when the boundary layer is laminar, it cannot be expected that the results obtained at any arbitrary Reynolds number with laminar boundary layers would correlate with results obtained with turbulent boundary layers.

In summary, it appears that the change in base pressure due to base bleed is primarily a function of and increases with the mass-flow ratio m_j/m_∞ when the velocity of base-bleed jets is subsonic. The larger the jet-area ratio, the higher the mass-flow ratio can be before the base-bleed jets attain sonic velocity. When the boundary layer approaching the trailing edge of the wing is turbulent, Reynolds number has only a secondary effect on the change in base pressure due to base bleed, and Mach number has essentially no effect. When the boundary layer is laminar, both Mach number and Reynolds number have secondary effects.

Effect of Base Bleed on the Drag of Blunt-Trailing-Edge Airfoils

From the data presented in figure 4, it is apparent that the base-bleed technique affords considerable reduction in the base drag of blunt-trailing-edge airfoils. The maximum reductions in base drag obtained with the half-blunt airfoil with turbulent boundary layers at a Mach number of 2 (see fig. 4(c)) are summarized below. The center column presents the ratio of the maximum change in base drag (corresponds to the peak base pressure) to the base drag without base bleed. The right-hand column presents the ratio of the maximum change in base drag to the total drag of the wing without base bleed.[1]

[1]The total drag was determined by adding the theoretical wave drag (from shock-expansion theory), the measured base drag, and an additional increment of drag coefficient of 0.0055 to account for turbulent skin friction.

$\frac{A_j}{A_b}$ percent	$\frac{c_{d_b} - c_{d_{bo}}}{c_{d_{bo}}}$ percent	$\frac{c_{d_b} - c_{d_{bo}}}{c_{d_o}}$ percent
25	-35.8	-11.4
50	-48.5	-15.5
75	-59.8	-19.1

From consideration of the base drag alone, the optimum jet-area ratio appears to be 1.0.

Unfortunately, the reduction in base drag resulting from base bleed is at least partially counteracted by the additional drag of the inlets and ducts required to entrain the bleed air. The usefulness of the base-bleed technique is dependent on the air induction drag being significantly less than the reduction in base drag. Since any reduction in the momentum of the base-bleed air between the inlet and the base of the airfoil will appear as an increase in total drag, it is evident that the inlet should be located in a region where the entering air has a relatively low momentum and the pressure is approximately ambient. In an attempt to arrive at a reasonable estimate for the air-induction drag, calculations have been made for a simple two-dimensional scoop that takes in low-energy boundary-layer air at the 80-percent-chord station of the half-blunt airfoil. The height of the scoop was adjusted to pass the desired mass-flow rate, assuming a turbulent boundary-layer profile. Sketches of the configuration considered, the details of the calculations, and the assumptions involved are contained in the Appendix. In brief, the reduction in total drag was calculated for varying mass-flow ratio through each of the double-jet nozzle blocks and with two different assumptions concerning the pressure acting on the back of the scoop. First, it was assumed that the flow separated from the back of the scoop and that the pressure in the separated region was equal to the base pressure without base bleed. Then it was assumed that the pressure over the back of the scoop was equal to the ambient static pressure. These two assumptions simulated approximately the maximum and minimum drag, respectively, that could result from the addition of the scoop to the basic airfoil profile. The maximum total drag reduction and the corresponding scoop height as indicated by these calculations for each of the nozzle blocks are tabulated below.

$\frac{A_j}{A_b}$	p_{b_o} acting on back of scoop			p_∞ acting on back of scoop		
	$\left(\frac{h_i}{h_b}\right)_{opt}$	$\frac{\Delta c_d}{c_{d_{b_o}}}$	$\frac{\Delta c_d}{c_{d_o}}$	$\left(\frac{h_i}{h_b}\right)_{opt}$	$\frac{\Delta c_d}{c_{d_{b_o}}}$	$\frac{\Delta c_d}{c_{d_o}}$
percent	percent	percent	percent	percent	percent	percent
25	8.4	-14	-4.5	9.0	-23	-7.2
50	6.3	-11	-3.6	8.1	-19	-6.0
75	5.1	-7.3	-2.3	7.4	-13	-4.2

These values do not correspond to the peak base pressure. The maximum reduction in total drag occurs at a lower mass-flow rate than that required for the maximum reduction in base drag. It can also be seen that the optimum scoop height decreases with increasing jet area. This is to be expected, since the closed area of the base decreases as the jet area increases and, hence, a given increase in base pressure corresponds to a smaller and smaller reduction in drag. Furthermore, since both the air-induction drag and the change in base drag must go to zero as the area ratio goes to zero, there must be an optimum area ratio somewhere below $A_j/A_b = 0.50$ for this inlet configuration and airfoil profile. For more efficient air-induction systems, the optimum jet area ratio would be larger.

To realize more worthwhile reductions in total drag, careful consideration must be given to the design of the air-induction system for each individual application. It would be desirable to utilize surplus air from some other system on the aircraft and thereby reduce the air induction drag chargeable to the bleed system to practically zero. For example, it might be practical to provide ducts from the boundary-layer removal slots of the engine inlet system to the plenum chamber of the base-bleed system. Another possibility would be to combine the base-bleed and boundary-layer-control techniques by utilizing the low pressure region at the base of a blunt-trailing-edge airfoil as a pump for boundary-layer suction on the surface of the wing.

CONCLUSIONS

Results obtained for a full-blunt and a half-blunt airfoil at Mach numbers of 1.5 and 2.0 indicate the following:

1. The base drag of blunt-trailing-edge airfoils can be reduced considerably (order of 50 percent) by bleeding relatively small quantities of air to the semidead-air region at the trailing edge of the airfoil.

2. The conditions for maximum base-drag reduction are:

(a) The bleed air should exhaust into the semidead-air region at subsonic velocity.

(b) The total pressure of the bleed air (plenum-chamber pressure) should be between 75 and 95 percent of the ambient static pressure.

(c) Although the effects of jet geometry and location were relatively small, jets located near the upper and lower edges of the base of the blunt-trailing-edge airfoil gave slightly better results than the other configurations tested.

(d) The mass-flow rate of the bleed air and, hence, the area of the jets should be as large as possible, consistent with requirements (a) and (b).

The reduction in base drag is counteracted by the drag of the air-induction system and these induction losses must be held to a minimum if worthwhile reductions in over-all drag are to be realized. General conclusions concerning the conditions for maximum reduction in total drag cannot be made without considering the design of the air-induction system.

Ames Aeronautical Laboratory
National Advisory Committee for Aeronautics
Moffett Field, Calif., Jan. 7, 1954

APPENDIX

REDUCTION IN TOTAL DRAG DUE TO BASE BLEED

The effectiveness of base bleed cannot be evaluated by considering only the reduction in base drag. The bleed air must be taken from the air stream and delivered to the base of the blunt-trailing-edge airfoil. Any change in the profile of the airfoil to accommodate an air inlet may result in a drag increase, and any reduction in the momentum of the bleed air between the inlet and the base of the airfoil will also increase the over-all drag. Thus, if Δc_d is the change in the total section drag due to base bleed, then

$$\Delta c_d = \Delta c_{d_b} + \Delta c_{d_f} + c_{d_i} \tag{A1}$$

where

Δc_{d_b} change in base drag due to base bleed

Δc_{d_f} change in foredrag due to the addition of an air inlet

c_{d_i} internal drag resulting from momentum losses of the bleed air

It is assumed that the airfoil profile without base bleed is as shown in sketch (a) and the profile with base bleed is as shown in sketch (b).

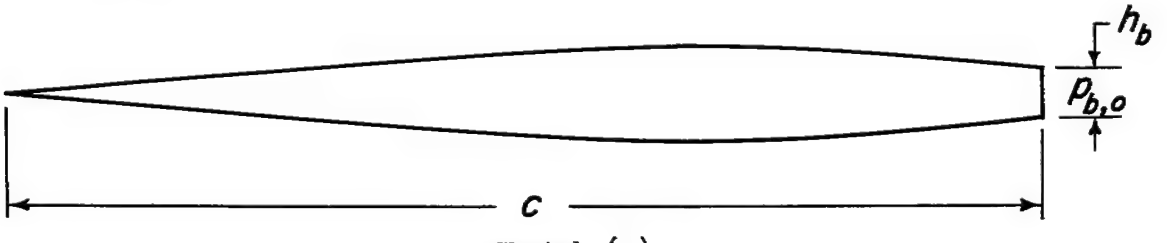

Sketch (a)

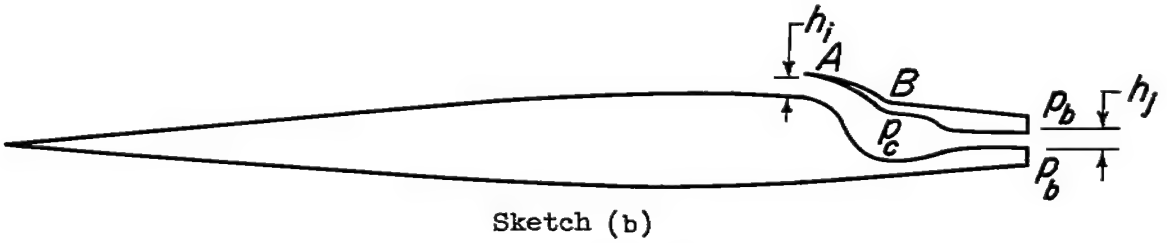

Sketch (b)

[redacted]

Then the change in base drag, taking into account the change in base area, is given by

$$\Delta c_{d_b} = -\frac{(p_b - p_\infty)(h_b - h_j)}{qc} + \frac{(p_{b_o} - p_\infty) h_b}{qc}$$

$$= \frac{p_\infty}{q}\left[\left(\frac{p_{b_o}}{p_\infty} - \frac{p_b}{p_\infty}\right)\frac{h_b}{c} + \left(\frac{p_b}{p_\infty} - 1\right)\frac{h_j}{c}\right] \qquad (A2)$$

To evaluate the change in foredrag, assumptions must be made concerning the air flow into and over the scoop. For simplicity, it is assumed that the height of the scoop is adjusted so that the mass-flow rate of the stream tube, bound by the surface of the airfoil and the streamline which coincides with the lip of the scoop, is equal to the mass-flow rate that the base-bleed nozzle will pass. In addition, it is assumed that the flow separates from the back of the scoop and that the pressure acting on the surface A-B is equal to the base pressure without base bleed, while the pressure acting on the surface from B to the trailing edge is unchanged by the addition of the scoop. This is believed to be a highly pessimistic assumption and, hence, leads to a conservative estimate of the total drag reduction. With these assumptions

$$\Delta c_{d_f} = -\frac{(p_{b_o} - p_\infty) h_i}{qc}$$

$$= -\frac{p_\infty}{q}\left(\frac{p_{b_o}}{p_\infty} - 1\right)\frac{h_i}{c} \qquad (A3)$$

The internal drag d_i can be evaluated by applying the momentum theorem on the dotted contour C shown in sketch (c).

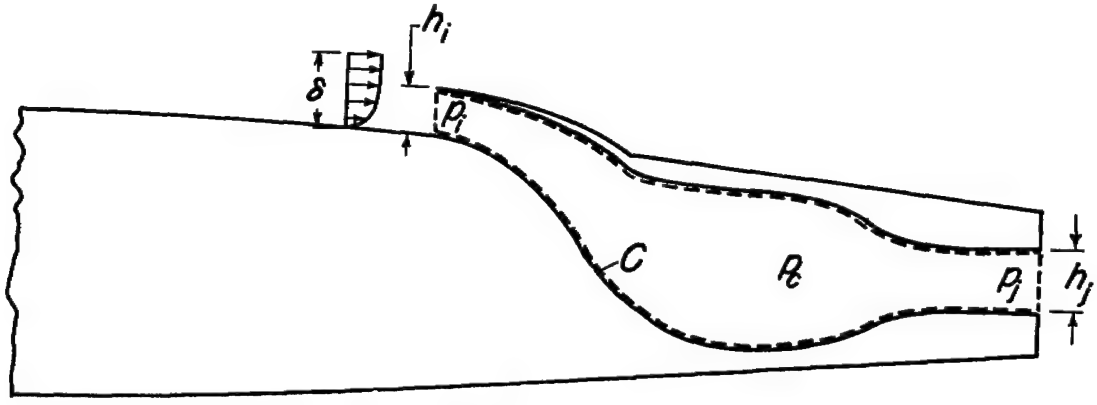

Sketch (c)

For two-dimensional, steady flow the momentum theorem may be expressed as follows:

$$\int_C \rho u V_n \, ds = -d_i - \int_{\substack{\text{inlet} \\ \text{and} \\ \text{exit}}} (p - p_\infty) \cos(n,x) \, ds \qquad (A4)$$

where

ρ mass density

u local velocity component in the x direction

V_n velocity normal to the contour

p static pressure

Since V_n is zero along the interior of the duct and assuming that the pressure is constant across the inlet and exit, equation (A4) may be written

$$d_i = (p_i - p_\infty) h_i - (p_j - p_\infty) h_j + \int_0^{h_i} \rho u^2 dy - \rho_j u_j^2 h_j \qquad (A5)$$

Since the mass-flow rate through the jet is given by

$$m_j = \rho_j u_j h_j$$

and the free-stream mass-flow rate through an area equal to the area of the base of the airfoil is given by

$$m_\infty = \rho_\infty u_\infty h_b$$

then equation (A5) may be rewritten in terms of the internal drag coefficient.

$$c_{d_i} = \frac{p_\infty}{q}\left[\left(\frac{p_i}{p_\infty} - 1\right)\frac{h_i}{c} - \left(\frac{p_j}{p_\infty} - 1\right)\frac{h_j}{c}\right] - 2\frac{u_j}{u_\infty}\frac{m_j}{m_\infty}\frac{h_b}{c} + 2\frac{\delta}{c}\int_0^{h_i/\delta} \frac{\rho}{\rho_\infty}\left(\frac{u}{u_\infty}\right)^2 d\frac{y}{\delta} \qquad (A6)$$

Combining equations (A1), (A2), (A3), and (A6), the equation for the change in total drag is obtained.

$$\Delta c_d = \frac{p_\infty}{q}\left[\left(\frac{p_{b_o}}{p_\infty} - \frac{p_b}{p_\infty}\right)\frac{h_b}{c} + \left(\frac{p_b}{p_\infty} - \frac{p_j}{p_\infty}\right)\frac{h_j}{c} + \left(\frac{p_i}{p_\infty} - \frac{p_{b_o}}{p_\infty}\right)\frac{h_i}{c}\right] -$$

$$2\,\frac{u_j}{u_\infty}\,\frac{m_j}{m_\infty}\,\frac{h_b}{c} + 2\,\frac{\delta}{c}\int_o^{h_i/\delta} \frac{\rho}{\rho_\infty}\left(\frac{u}{u_\infty}\right)^2 d\,\frac{y}{\delta} \qquad \text{(A7)}$$

Before equation (A7) can be applied to the experimental results, it is necessary to determine the height of the inlet h_i and to evaluate the integral term as functions of the mass-flow ratio m_j/m_∞. Since the mass-flow rate of the base-bleed jet must be equal to the mass flow through the inlet, the following equation can be written

$$\frac{m_j}{m_\infty} = \frac{m_i}{m_\infty} = \frac{1}{h_b}\int_o^{h_i} \frac{\rho}{\rho_\infty}\,\frac{u}{u_\infty}\,dy \qquad \text{(A8)}$$

In terms of the boundary-layer thickness δ at the inlet, equation (A8) becomes

$$\frac{m_j}{m_\infty} = \frac{\delta}{h_b}\int_o^{h_i/\delta} \frac{\rho}{\rho_\infty}\,\frac{u}{u_\infty}\,d\,\frac{y}{\delta}$$

when $h_i \leq \delta$ or

$$\frac{m_j}{m_\infty} = \frac{\delta}{h_b}\left[\int_o^1 \frac{\rho}{\rho_\infty}\,\frac{u}{u_\infty}\,d\,\frac{y}{\delta} + \left(\frac{h_i}{\delta} - 1\right)\right] \qquad \text{(A9)}$$

when $h_i > \delta$.

For a thin airfoil section at zero angle of attack, the Mach number of the flow just outside the boundary layer at the 80-percent-chord station would be close to the free-stream Mach number M_∞. For the purpose of these calculations, it was assumed that the Mach number and velocity outside the boundary layer at this point were the same as in the undisturbed stream. In addition, it was assumed that the boundary layer at this station was turbulent and that the velocity profile was given by

$$\frac{u}{u_\infty} = \left(\frac{y}{\delta}\right)^{1/7}$$

Finally, it was assumed that the Prandtl number was unity and, therefore,

$$\frac{\rho}{\rho_\infty} = \frac{1}{1 + \frac{\gamma-1}{2} M_\infty^2 \left[1 - \left(\frac{u}{u_\infty}\right)^2\right]}$$

Substituting these relations into equation (A9) and integrating gives the following results:

when $\frac{h_i}{\delta} < 1$

$$\frac{m_j}{m_\infty} = \frac{\delta}{h_b} \frac{7}{2b} \left\{ \left(\frac{1+b}{b}\right)^3 \log \left[\frac{1+b}{(1+b) - b\left(\frac{h_i}{\delta}\right)^{2/7}} \right] - \left(\frac{1+b}{b}\right)^2 \left(\frac{h_i}{\delta}\right)^{2/7} - \frac{1}{2}\left(\frac{1+b}{b}\right)\left(\frac{h_i}{\delta}\right)^{4/7} - \frac{1}{3}\left(\frac{h_i}{\delta}\right)^{6/7} \right\}$$

when $\frac{h_i}{\delta} \geq 1$

$$\frac{m_j}{m_\infty} = \frac{\delta}{h_b} \left\{ \left(\frac{h_i}{\delta} - 1\right) + \frac{7}{2b} \left[\left(\frac{1+b}{b}\right)^3 \log (1+b) - \left(\frac{1+b}{b}\right)^2 - \frac{1}{2}\left(\frac{1+b}{b}\right) - \frac{1}{3} \right] \right\} \tag{A10}$$

where $b = \frac{\gamma-1}{2} M_\infty^2$

With these same assumptions the integral term of equation (A7) may be expressed as follows:

when $\frac{h_i}{\delta} < 1$

$$\int_0^{h_i/\delta} \frac{\rho}{\rho_\infty}\left(\frac{u}{u_\infty}\right)^2 d\,\frac{y}{\delta} = \frac{7}{2\sqrt{b\,(1+b)}}\left(\frac{1+b}{b}\right)^4 \log \frac{\sqrt{1+b} + \sqrt{b}\left(\frac{h_i}{\delta}\right)^{1/7}}{\sqrt{1+b} - \sqrt{b}\left(\frac{h_i}{\delta}\right)^{1/7}} -$$

$$\frac{7}{b}\left[\left(\frac{1+b}{b}\right)^3\left(\frac{h_i}{\delta}\right)^{1/7} + \frac{1}{3}\left(\frac{1+b}{b}\right)^2\left(\frac{h_i}{\delta}\right)^{2/7} + \right.$$

$$\left.\frac{1}{5}\left(\frac{1+b}{b}\right)\left(\frac{h_i}{\delta}\right)^{5/7} + \frac{1}{7}\left(\frac{h_i}{\delta}\right)\right]$$

when $\frac{h_i}{\delta} \geq 1$

$$\int_0^{h_i/\delta} \frac{\rho}{\rho_\infty}\left(\frac{u}{u_\infty}\right) d\,\frac{y}{\delta} = \left(\frac{h_i}{\delta} - 1\right) + \frac{7}{2\sqrt{b\,(1+b)}}\left(\frac{1+b}{b}\right)^4 \log \frac{\sqrt{1+b} + \sqrt{b}}{\sqrt{1+b} - \sqrt{b}} -$$

$$\frac{7}{b}\left[\left(\frac{1+b}{b}\right)^3 + \frac{1}{3}\left(\frac{1+b}{b}\right)^2 + \frac{1}{5}\left(\frac{1+b}{b}\right) + \frac{1}{7}\right] \qquad \text{(A11)}$$

The mass-flow ratio m_j/m_∞ was determined experimentally and the boundary-layer thickness δ at the inlet was calculated by the method of reference 4. With these values, the height of the inlet h_i was determined from equation (A10) for each experimental point. Equations (A7) and (A11) and the corresponding experimental data were then employed to determine the reduction in total drag for that particular set of test conditions. An additional group of calculations were made assuming that the pressure acting on the back of the scoop was equal to the ambient static pressure. With this assumption, the change in foredrag Δc_{d_f} as given by equation (A3) was zero and equation (A7) was changed accordingly.

REFERENCES

1. Chapman, Dean R.: Airfoil Profiles for Minimum Pressure Drag at Supersonic Velocities - General Analysis with Application to Linearized Supersonic Flow. NACA Rep. 1063, 1952. (Formerly NACA TN 2264)

2. Chapman, Dean R., and Kester, Robert H.: Effect of Trailing-Edge Thickness on Lift at Supersonic Velocities. NACA RM A52D17, 1952.

3. Cortright, Edgar M., Jr., and Schroeder, Albert H.: Preliminary Investigation of Effectiveness of Base Bleed in Reducing Drag of Blunt-Base Bodies in Supersonic Stream. NACA RM E51A26, 1951.

4. Van Driest, E. R.: Turbulent Boundary Layer in Compressible Fluids. Jour. Aero. Sci., vol. 18, no. 3, Mar. 1951, pp. 145-160, 216.

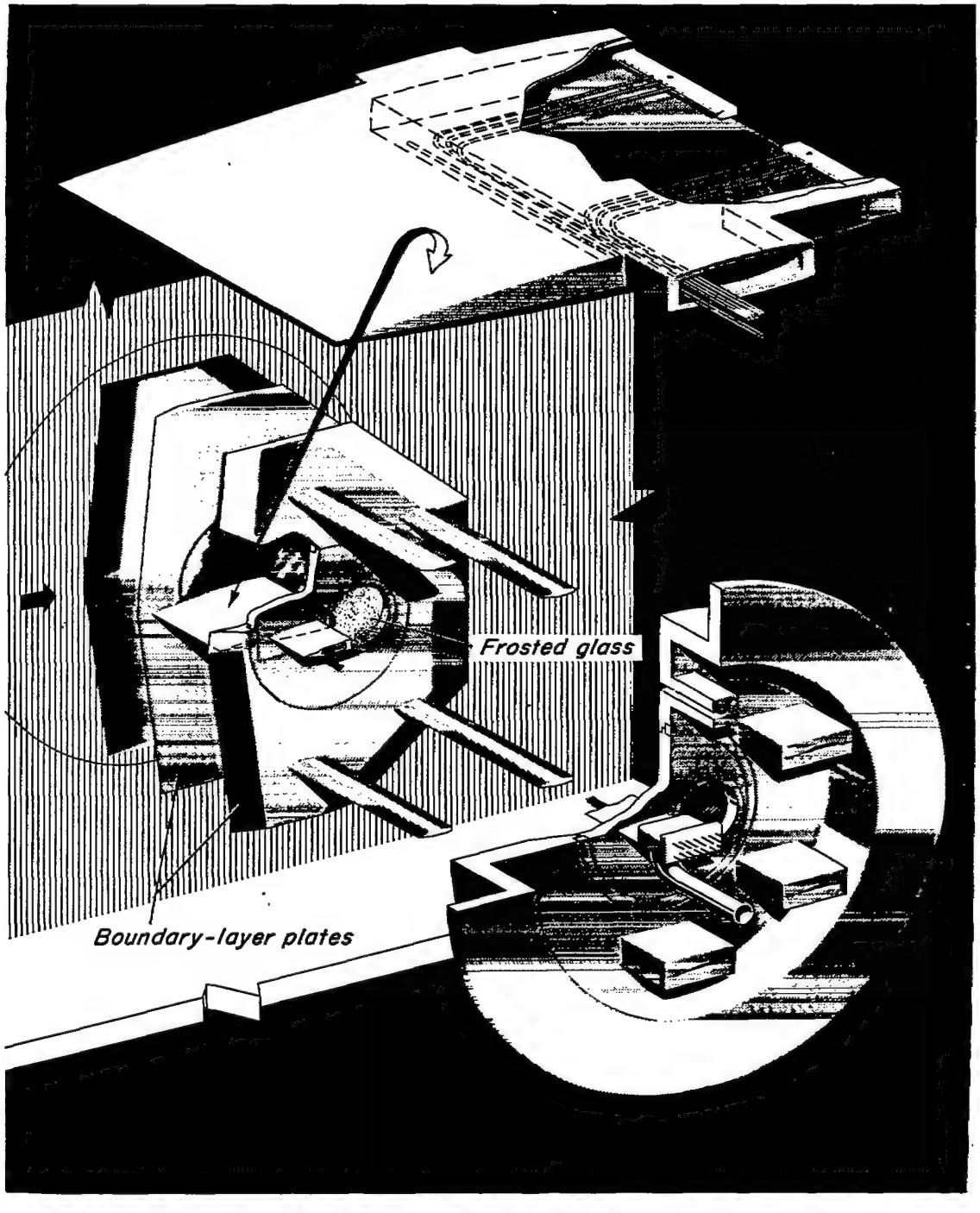

A-18802

Figure 1.- The half-blunt airfoil model installed in the two-dimensional channel.

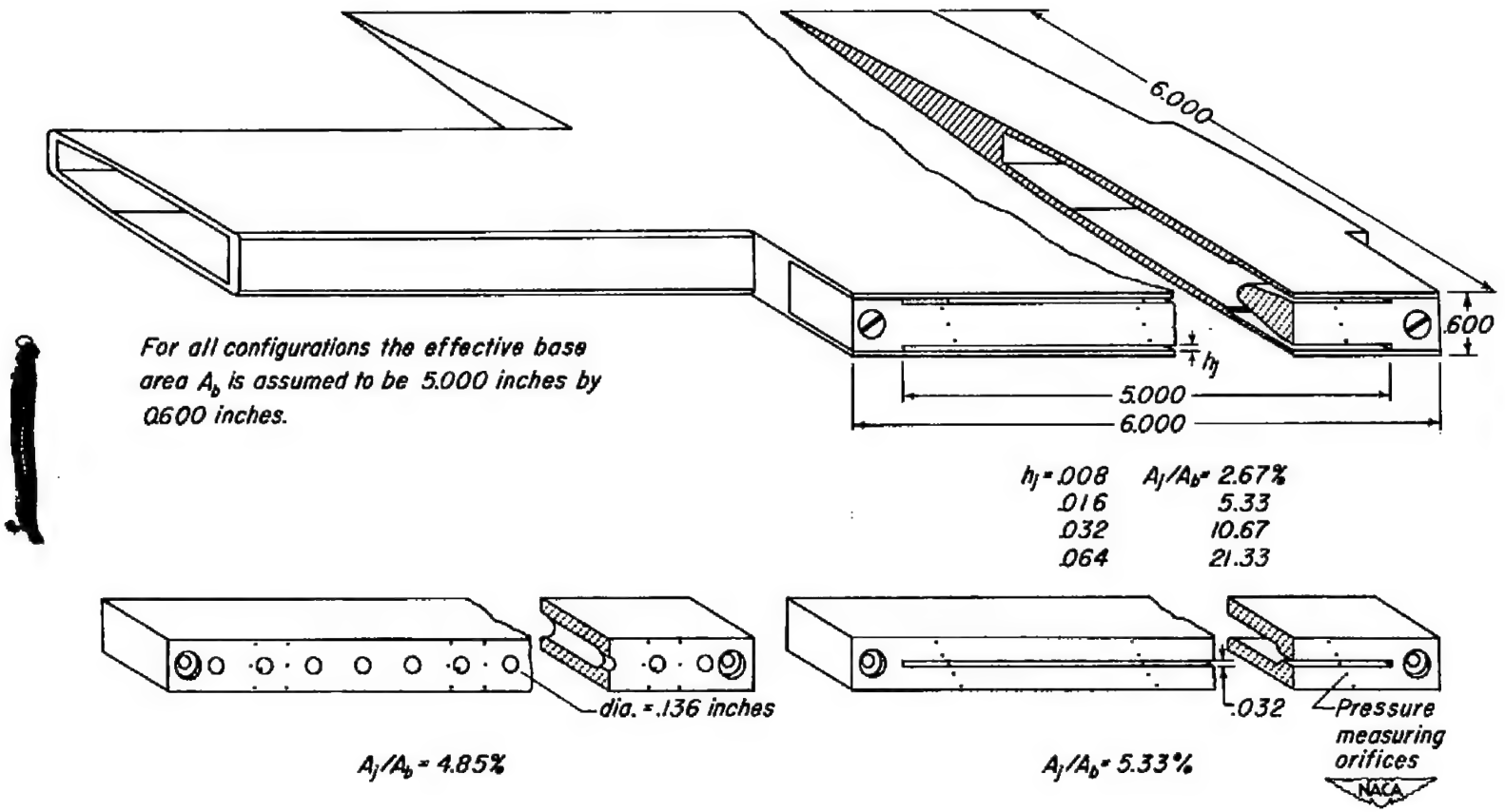

(a) The full-blunt airfoil.

Figure 2.- The airfoil models and base blocks used in the investigation.

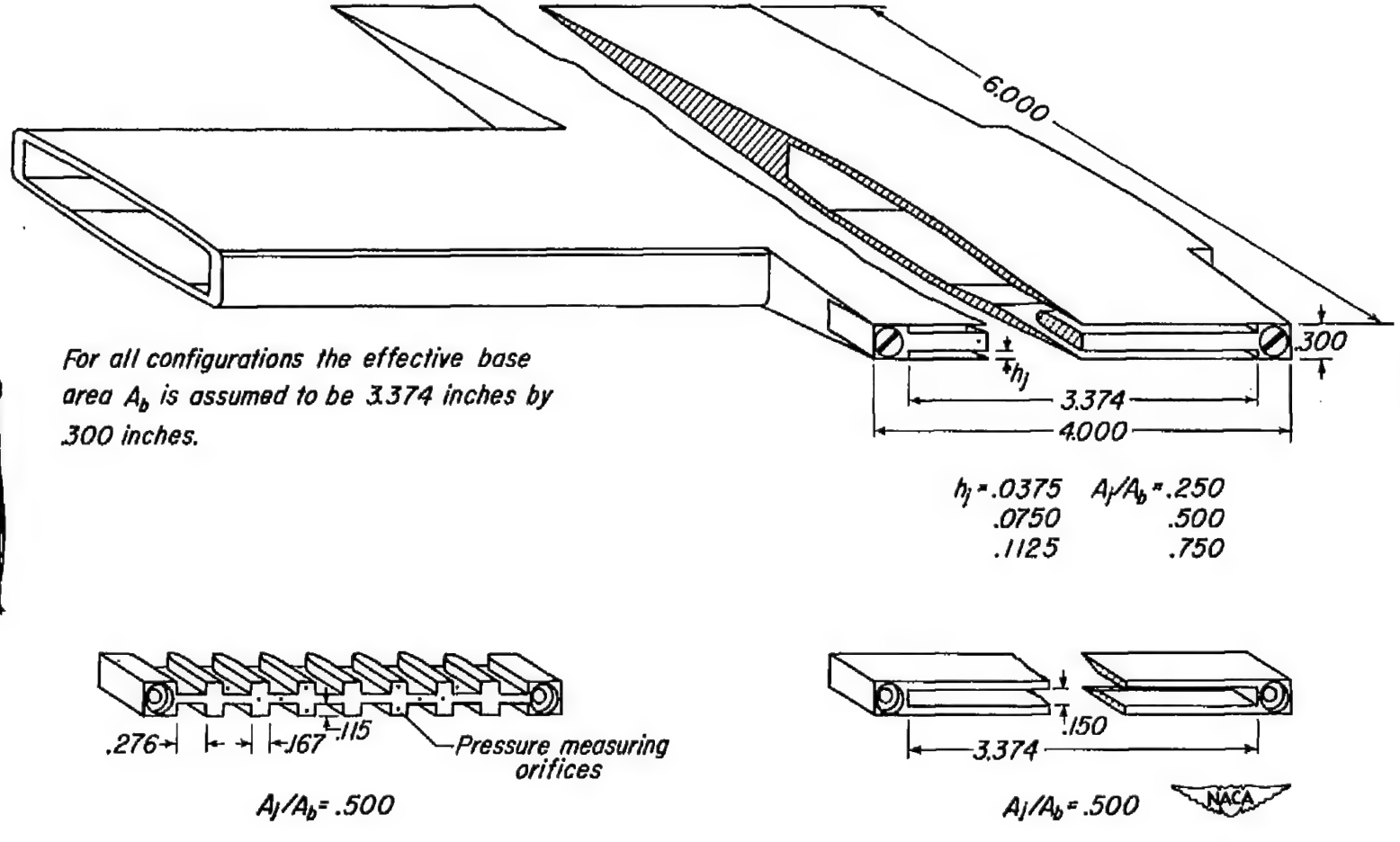

(b) The half-blunt airfoil.

Figure 2.- Concluded.

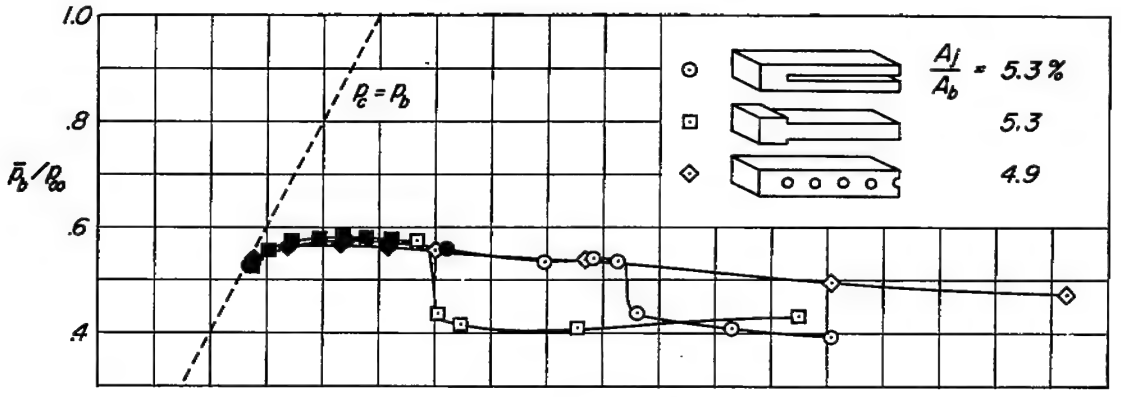

(a) Full-blunt wing, turbulent boundary layer, M = 1.5, R = 2.7×10^6.

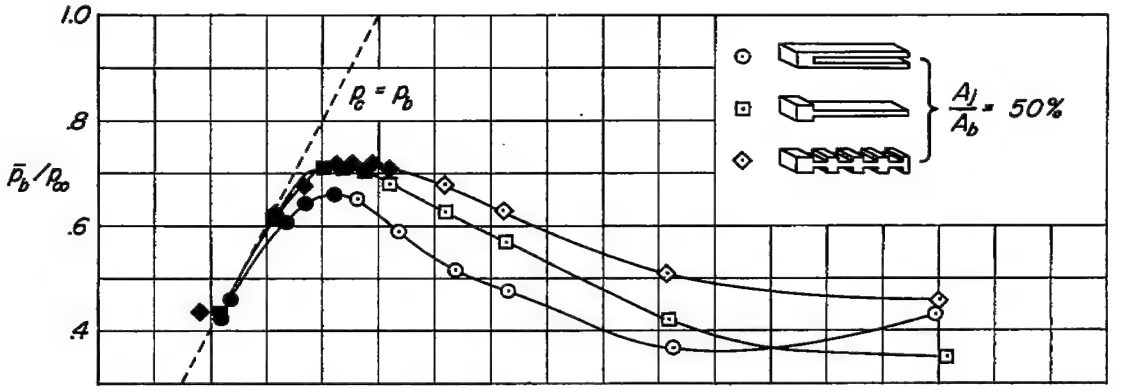

(b) Half-blunt wing, turbulent boundary layer, M = 2.0, R = 3.1×10^6.

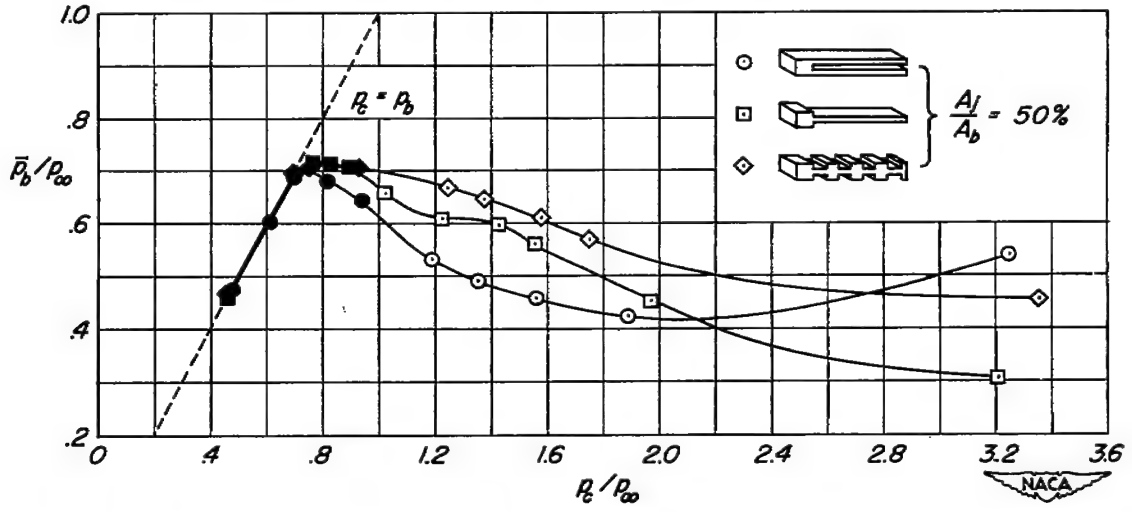

(c) Half-blunt wing, laminar boundary layer, M = 2.0, R = 1.2×10^6.

Figure 3.- Effect of jet geometry on the variation of base pressure with chamber pressure.

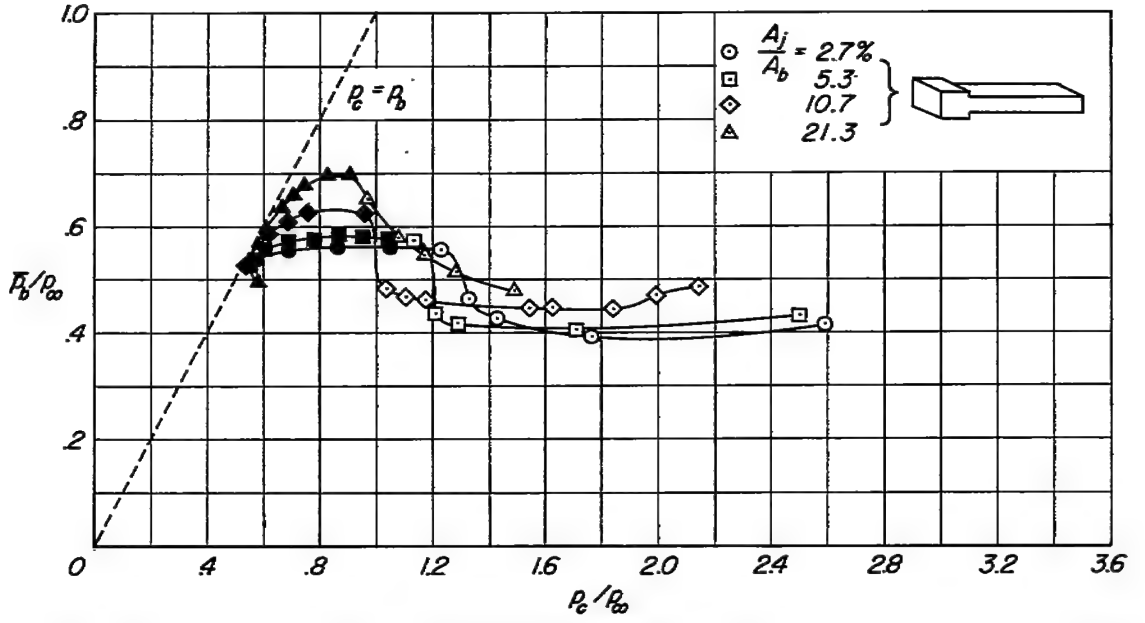

(a) Full-blunt wing, turbulent boundary layer, M = 1.5, R = 2.7×10^6.

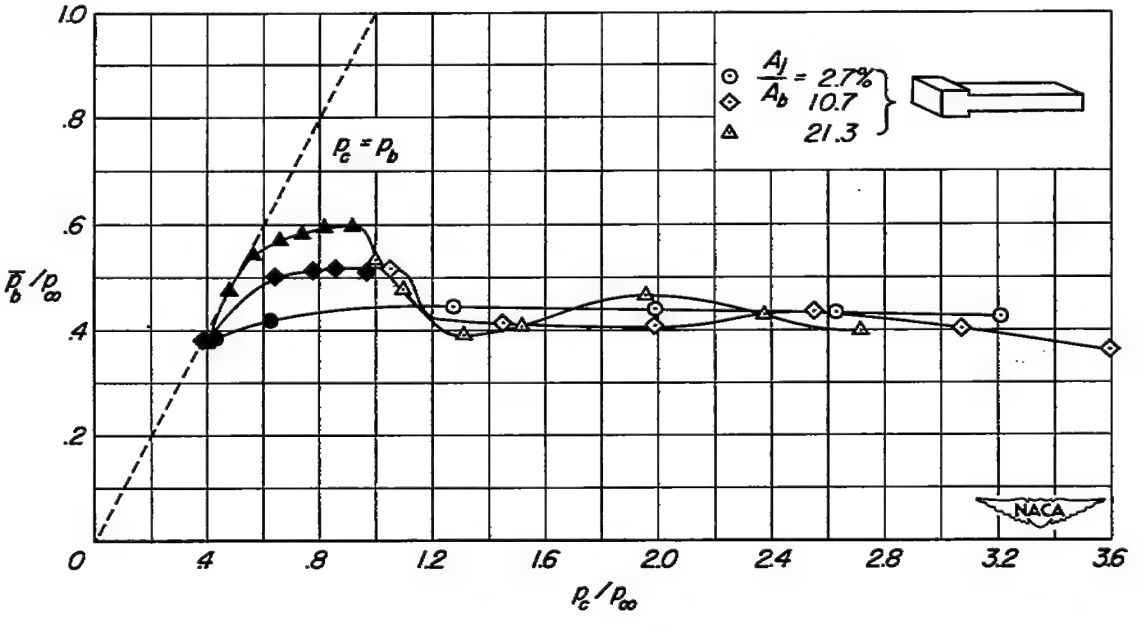

(b) Full-blunt wing, turbulent boundary layer, M = 2.0, R = 2.7×10^6.

Figure 4.- Effect of jet area on the variation of base pressure with chamber pressure.

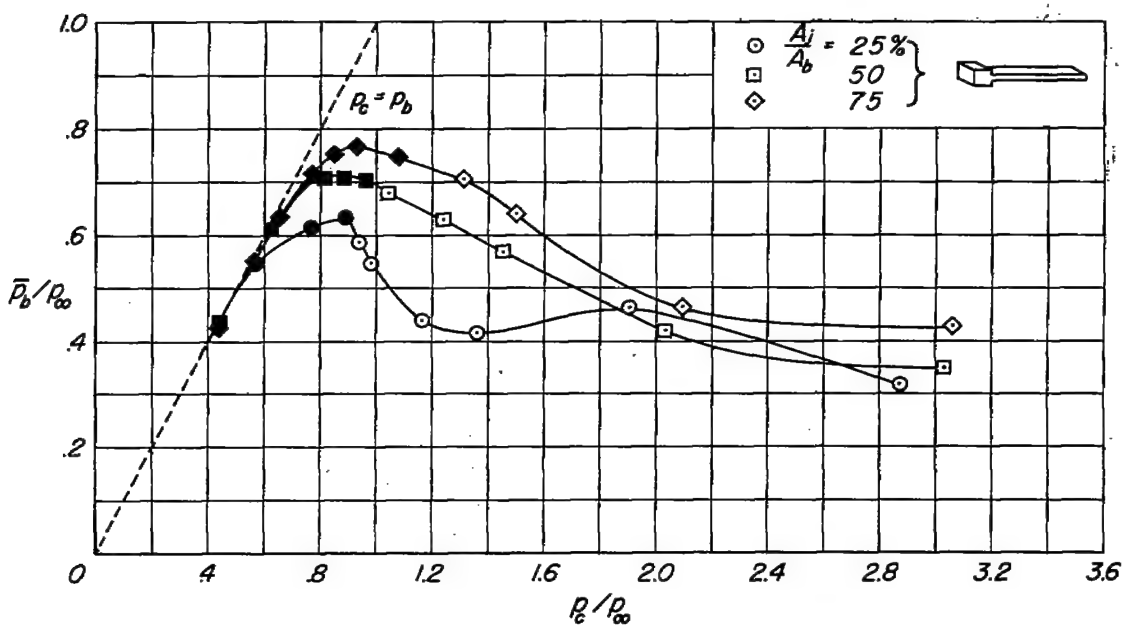

(c) Half-blunt wing, turbulent boundary layer, M = 2.0, R = 3.1×10^6.

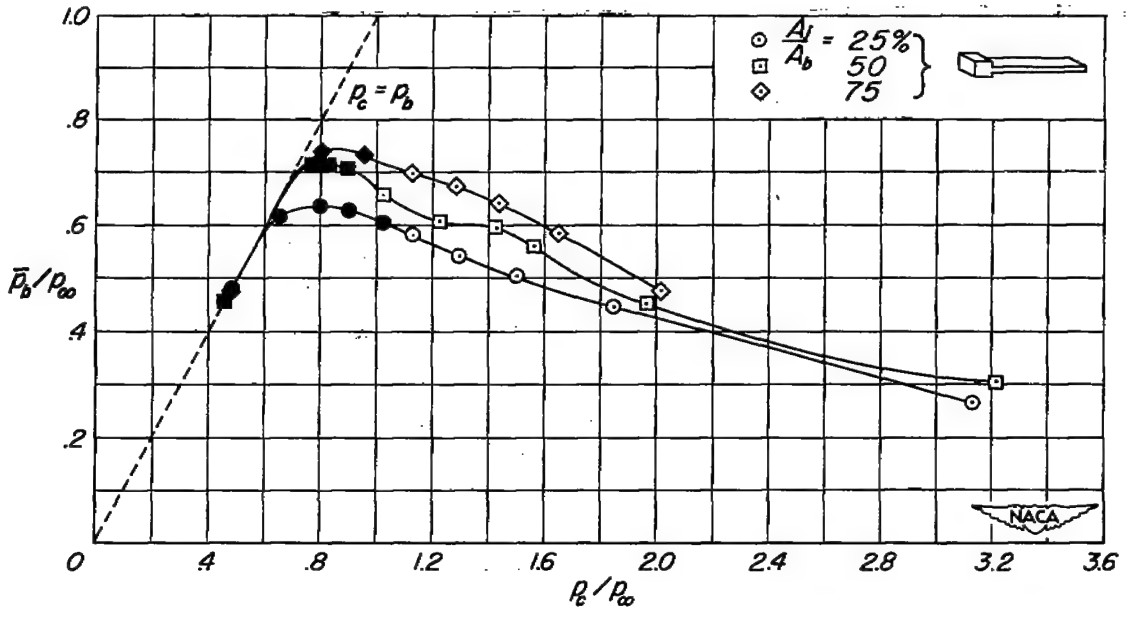

(d) Half-blunt wing, laminar boundary layer, M = 2.0, R = 1.2×10^6.

Figure 4.- Concluded.

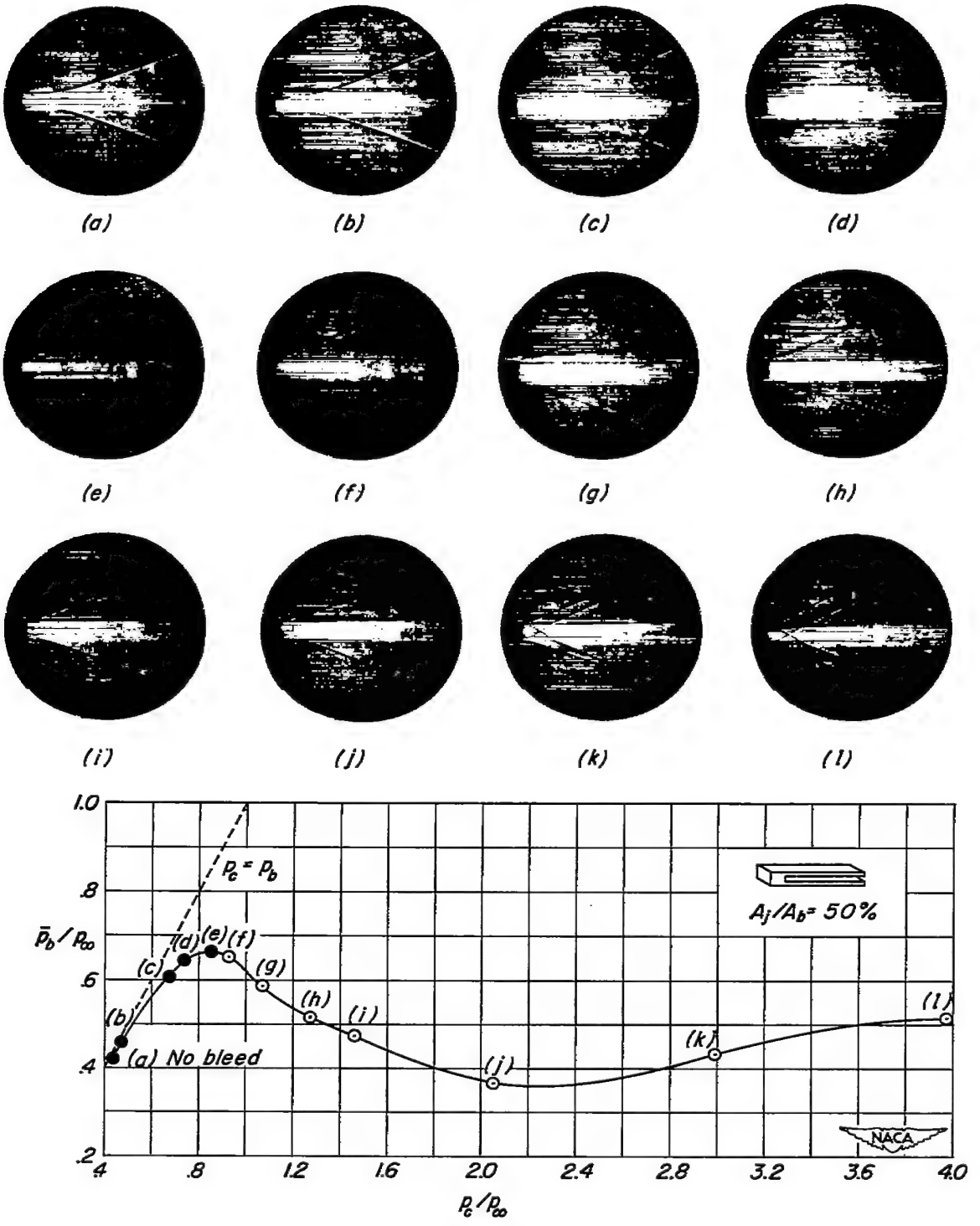

Figure 5.- Shadowgraph pictures of the wake behind the half-blunt wing with a single jet nozzle. Turbulent boundary layer, M = 2.0, $R = 3.1 \times 10^6$.

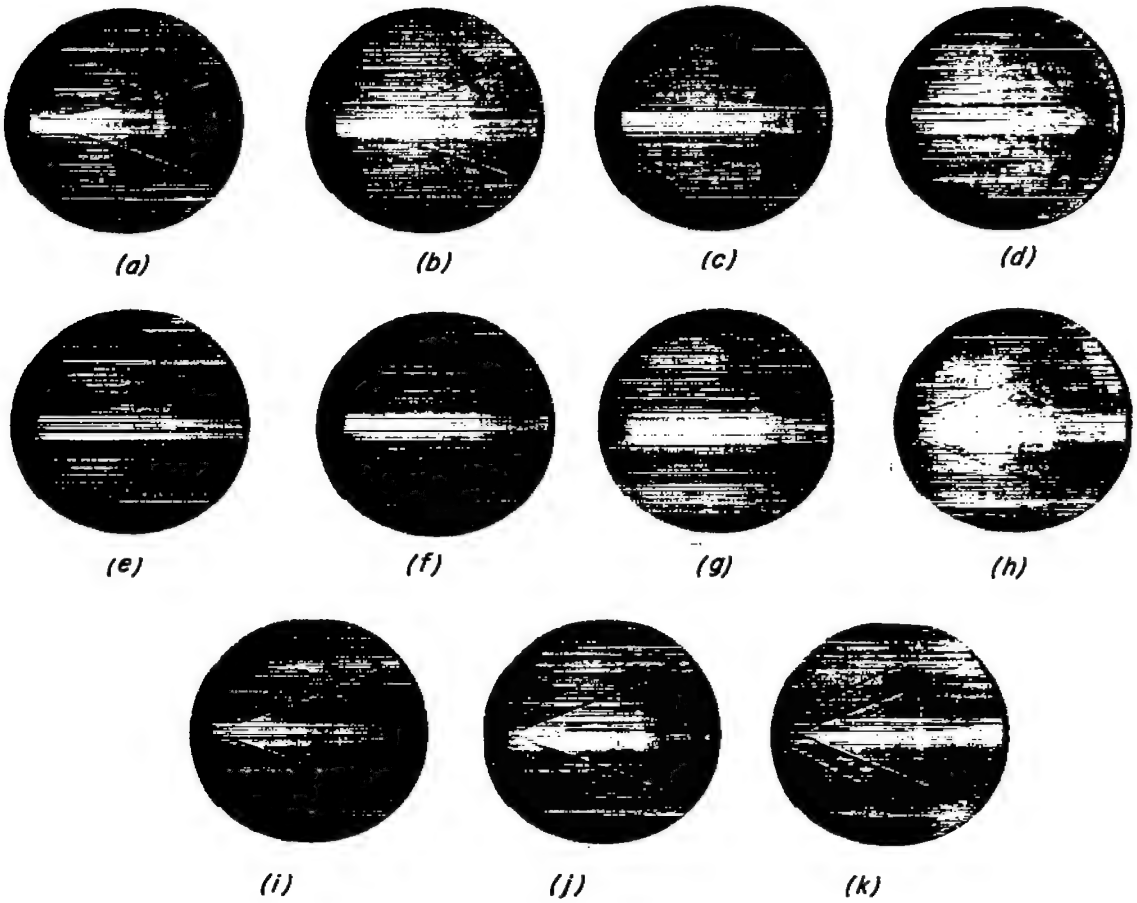

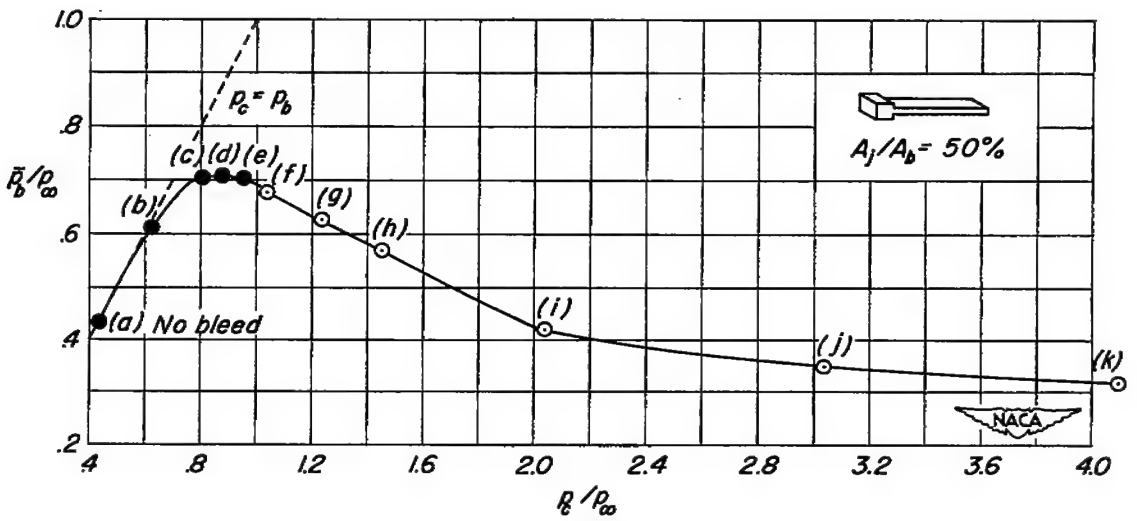

Figure 6.- Shadowgraph pictures of the wake behind the half-blunt wing with a double jet nozzle. Turbulent boundary layer, M = 2.0, R = 3.1×10^6.

[redacted]

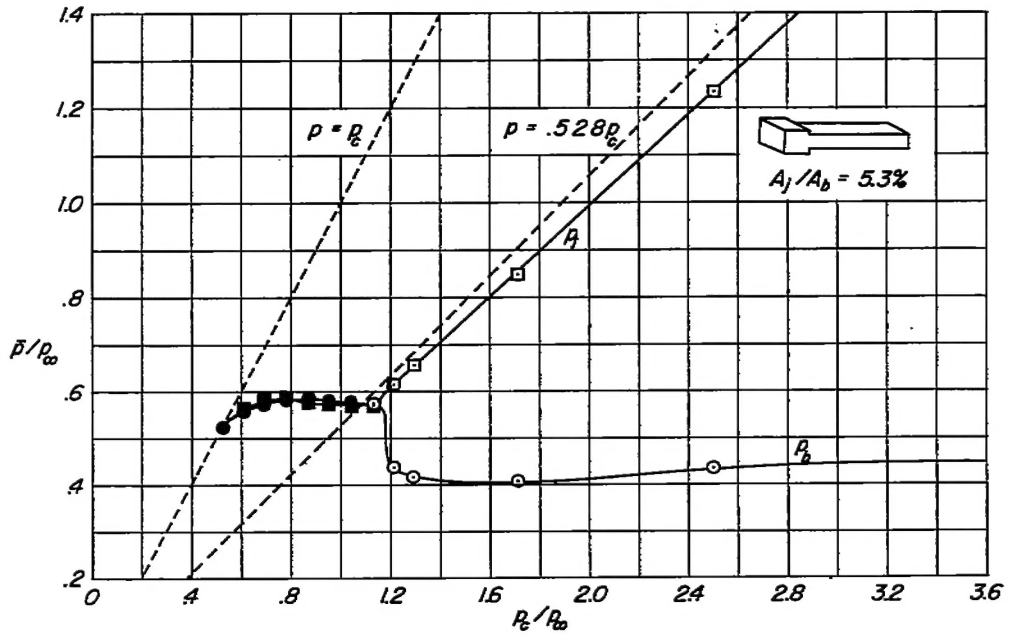

(a) Full-blunt wing, turbulent boundary layer, M = 1.5x10^6, R = 2.7x10^6.

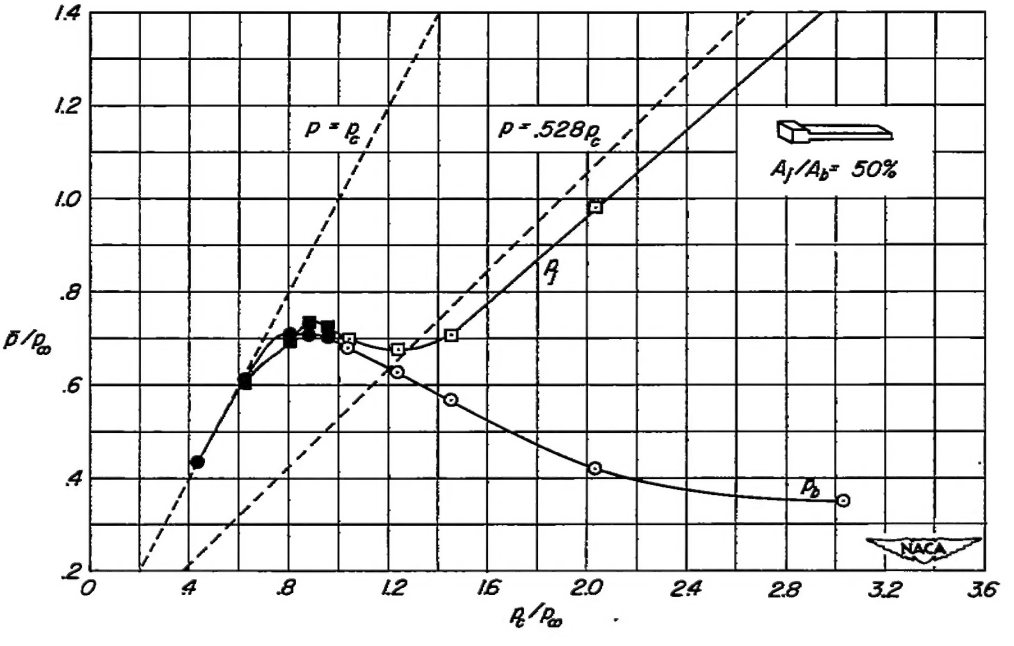

(b) Half-blunt wing, turbulent boundary layer, M = 2.0, R = 3.1x10^6.

Figure 7.- Examples of the two types of results associated with sonic flow through the nozzles.

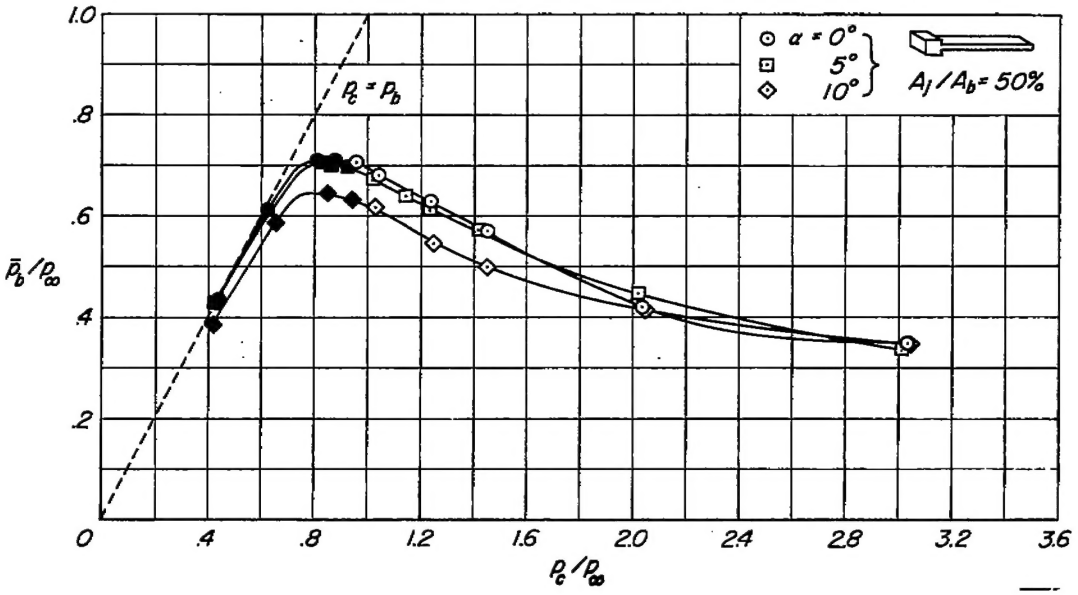

Figure 8.- Effect of angle of attack on the variation of base pressure with chamber pressure. Half-blunt wing, turbulent boundary layer, M = 2.0, R = 3.1×10^6.

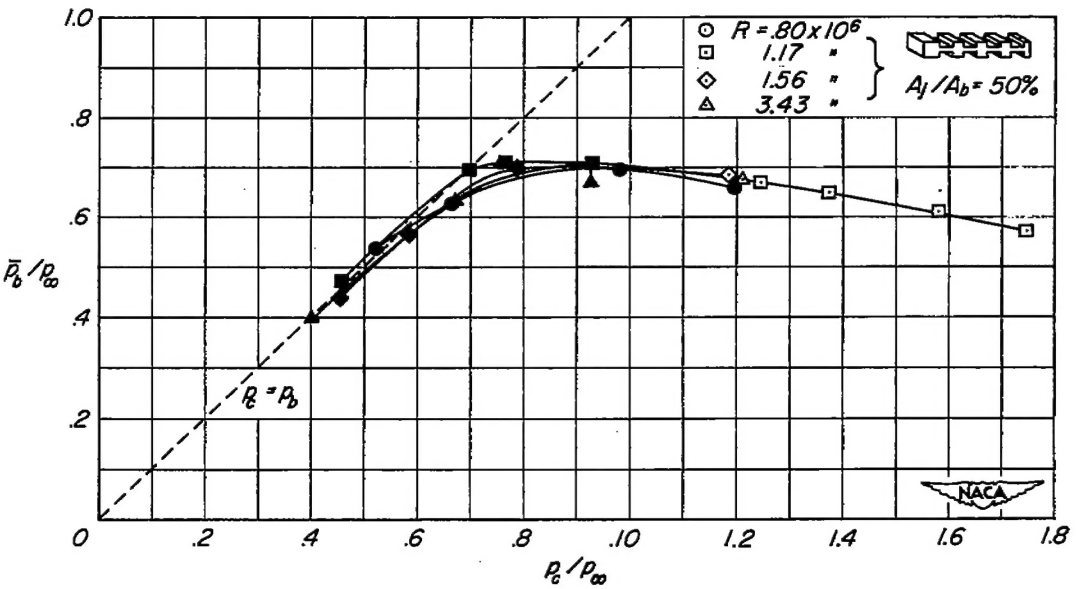

Figure 9.- Effect of Reynolds number on the variation of base pressure with chamber pressure. Half-blunt wing, M = 2.0.

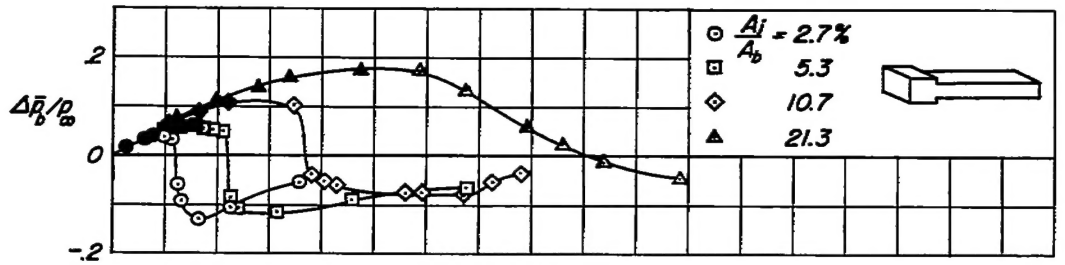

(a) Full-blunt wing, turbulent boundary layer, M = 1.5, R = 2.7×10^6.

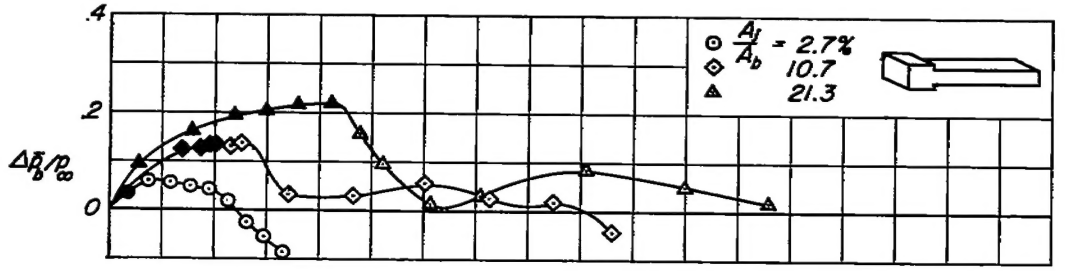

(b) Full-blunt wing, turbulent boundary layer, M = 2.0, R = 2.7×10^6.

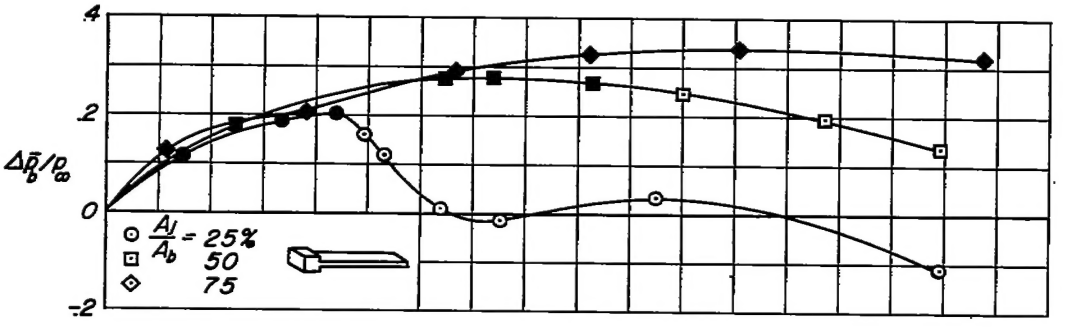

(c) Half-blunt wing, turbulent boundary layer, M = 2.0, R = 3.1×10^6.

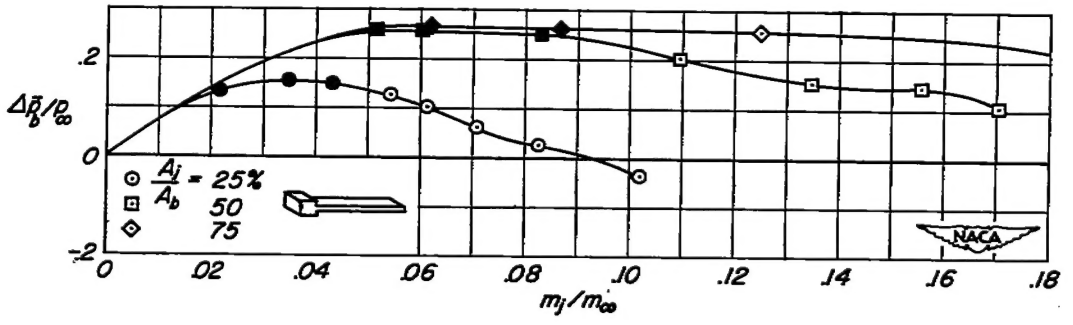

(d) Half-blunt wing, laminar boundary layer, M = 2.0, R = 1.2×10^6.

Figure 10.- The change in base pressure as a function of mass-flow rate through the jets.

[redacted]